Quantum-well states and magnetic coupling between ferromagnets through a noble-metal layer

J. E. Ortega and F. J. Himpsel
IBM Research Division, Thomas J. Watson Research Center, P.O. Box 218, Yorktown Heights, New York 10598

G. J. Mankey and R. F. Willis
Physics Department, Pennsylvania State University, University Park, Pennsylvania 16802
(Received 18 May 1992; revised manuscript received 9 September 1992)

Using inverse photoemission and photoemission we find that the bulk bands become discretized in highly perfect layer structures, such as Cu on fcc Co(100), Cu on fcc Fe(100), Ag on bcc Fe(100), Au on bcc Fe (100), fcc Co on Cu(100), and bcc Fe on Au(100). The electronic structure is analyzed in the framework of quantum-well states consisting of bulk Bloch functions modulated by an envelope function. The wavelength of the envelope function is determined from the $\lambda/2$ interferometer fringes produced by the periodic appearance of quantum-well states with increasing film thickness. Using k conservation, one obtains an absolute measurement of the band dispersion for the s,p bands of Fe, Cu, Ag, and Au. Quantum-well states at the Fermi level are found to be closely connected with oscillatory magnetic coupling in superlattices. They are spin polarized, even in noble metals, due to the spin-dependent band structure of the confining ferromagnet. The oscillation period is half the wavelength of the envelope function. The corresponding wave vector is given by the Fermi wave vector and by the wave vector of the nearest s,p band edge via $2(k_{\rm edge}-k_F)$. This turns out to be equivalent to Ruderman-Kittel-Kasuya-Yosida theory.

I. INTRODUCTION

The general goal of our work is to measure the changes in the electronic structure of solids as one goes from the bulk to thin films, superlattices, and ultimately to a monolayer.[1,2] In an attempt to reach the atomic limit, we place emphasis on structures that can be designed layer by layer. Indeed, the effects discussed here require atomically smooth films. Particular attention will be paid to magnetic effects in thin-film structures, such as oscillatory magnetic coupling in superlattices and spin valves.[3–18] These structures have created widespread interest, due to their potential applications in magnetic storage as well as to basic questions raised by surprisingly long oscillation periods. A number of theoretical studies[19–25] deal with the question of magnetic coupling between ferromagnetic layers across a nonmagnetic spacer layer. Our intention is to visualize the electronic states involved in the coupling, and thus to understand intuitively some puzzling questions, such as why a noble-metal spacer can transmit magnetic coupling over distances of up to 20 layers, having only nonmagnetic, s,p electrons available at the Fermi level, and why typical oscillation periods of the magnetic coupling are as large as six layers, while a naive model would predict oscillations with twice the period of the Fermi wave vector, which is of atomic dimensions. For this purpose we will pay particular attention to thin-film states at the Fermi level, which determine magnetic coupling and transport.

In the following, we will begin by demonstrating $k^{\perp}$ quantization in thin-film structures in Sec. II, using angle-resolved photoemission and inverse photoemission to probe occupied and unoccupied electronic states. Section II A discusses how the band offsets between noble metals and transition metals determine the confinement of electronic states to a thin film. Preparation methods are given in Sec. II B, since it is critical to prepare atomically smooth films in order to see discrete layer states at all. The wave functions of thin-film states are explained in Sec. III, using the formalism developed for quantum-well states. Essentially, a bulk Bloch function is modulated by a slowly varying envelope function, which ensures that the boundary conditions are met at the interfaces. It is shown in Sec. III A how the wavelength of the envelope function can be obtained directly from oscillations of the inverse photoemission intensity with film thickness, which are analogous to interference fringes in a Fabry-Perot interferometer. In Sec. III B this information is used to demonstrate an absolute method for determining band dispersions. Section III C deals with quantum wells approaching the monolayer limit, where the atoms in the quantum well cease to exhibit bulklike behavior, due to the change in bonding across the interface. Having clarified the nature of electronic states in thin films of ferromagnets and noble metals, we proceed in Sec. IV to explore the implications for oscillatory magnetic coupling in multilayers of a ferromagnet and a noble metal. We present evidence in Sec. IV A that magnetic coupling is transmitted through the noble metal by spin-polarized quantum-well states at the Fermi level. Its periodicity is determined by the envelope function, as shown in Sec. IV B. The corresponding wave vector is given by $2(k_{\rm edge}-k_F)$, averaged over all parallel wave vectors $k^{\parallel}$, where $k_{\rm edge}$ are wave vectors of the s,p band edges closest to the Fermi wave vectors k_F. This turns out to be equivalent to Ruderman-Kittel-Kasuya-Yosida (RKKY) theory. For the (100) orientation the expression reduces to $2(k_{\rm ZB}-k_F)$, which can be understood as a

beating frequency between the RKKY frequency $2k_F$ and the lattice periodicity $2k_{ZB}$. While the oscillation period is determined by the band structure of the noble-metal spacer, its phase is given by bands of the ferromagnet, as explained in Sec. IV C.

II. QUANTIZATION OF $k^\perp$ IN THIN FILMS

In general, one would expect electronic states to become discretized by confining them in the direction perpendicular to a thin film. This is borne out by many band-structure calculations performed for finite slabs. Figure 1 gives an example showing the band structure of an eleven-layer Ag(100) film[26] compared to the bulk-band structure[27] of Ag along the [100] direction. For our data, taken at $k^\parallel=0$, we focus on the s,p band at $\bar{\Gamma}_1$ in the slab calculation, which corresponds to the $\Gamma_{12}\Delta_1 X_4'$ line in the bulk. The continuous Δ_1 band splits up into discrete points in the slab. Their number increases with the number of layers. Exactly such a behavior is observed for thin-metal films [Figs. 2(a)–2(h), 3(a)–3(d), and Refs. 1 and 2; for other work on finite-size effects in metals see Refs. 28–35]. Taking as an example the series of spectra for Cu on fcc Fe(100) in Fig. 2(b), we can see that the nearly structureless spectrum of bulk Cu(100) at the top breaks up into a series of peaks for thin films. These structures move systematically to higher energy with increasing film thickness, as can be seen more easily in the structure plot in Fig. 3(b). They eventually converge toward the top of the s,p band at X_4'. This critical point shows up in the bulk-Cu(100) spectrum as an intensity cutoff at around 1.8 eV (compare also Ref. 36). Such a behavior is easily understood from the band-structure diagram in Fig. 1. With increasing film thickness, the spacing between the discrete $k^\perp$ points decreases. Therefore, all states appear to move toward the upper band edge X_4', if we start numbering them from the top down, as done in our figures.

A. Criteria for the existence of discrete states

The discrete thin-film states behave qualitatively the same way in all structures studied here, i.e., fcc Cu on fcc Co(100) and on fcc Fe(100), fcc Ag and fcc Au on bcc Fe(100), fcc Co on fcc Cu(100), and bcc Fe on fcc Au(100). In all cases, we are dealing with a Δ_1 s,p band dispersing upward through the Fermi level toward a maximum at the Brillouin-zone boundary (X_4' for fcc and H_{15} for bcc lattices in the [100] direction). Inverse photoemission is particularly useful in understanding the systematics of these thin-film states, since one can see them converge toward the unoccupied s,p band edge with increasing film thickness.

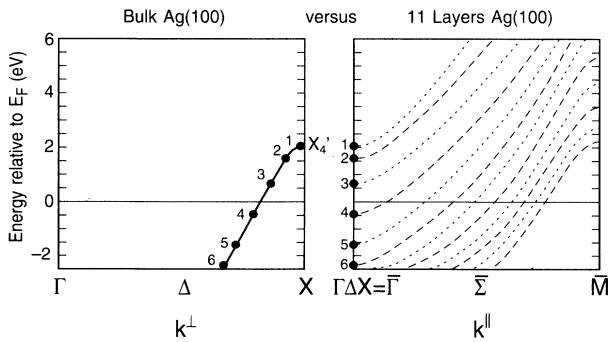

FIG. 1. Discretization of the perpendicular wave vector $k^\perp$ in a thin film, demonstrated by a band calculation (Ref. 26) for an eleven-layer Ag(100) slab (right-hand side). The discrete states of the slab calculation (dots) are mapped onto a bulk-band calculation (Ref. 27) (left-hand side).

A more detailed look at the relative locations of substrate versus overlayer bands reveals distinct differences between noble metals on ferromagnets and ferromagnets on noble metals. The s,p band of noble metals generally lies lower than that of $3d$ ferromagnets with the same structure, as determined in detail in a separate study.[37] The relative band arrangement has consequences for the existence and dimensionality of thin-film states. Ferromagnets on noble metals, e.g., fcc Co on Cu(100), exhibit truly two-dimensional thin-film states near the top of the s,p band, because the wave function has no states in the substrate to connect with and is completely Bragg reflected. This is confirmed by the absence of $k^\perp$ dispersion when changing the initial energy in inverse photoemission. In the reverse case, e.g., for Cu on fcc Co(100) and on fcc Fe(100), the wave function is only partially reflected at the interface and can couple to the three-dimensional s,p band of the substrate, thereby forming a resonance. The empirical fact that we do see strong, discrete states even in the second case shows that the reflectivity must be rather high, giving rise to a strong standing wave in the overlayer and only a small leakage into the substrate. We suspect that the higher-lying s,p band in the ferromagnet represents a barrier in the average potential relative to the noble metal. Such a potential step may provide enough reflectivity to observe discrete thin-film resonances.

Up to now, we have left out the d bands that are present near the Fermi level in ferromagnets. For the high-symmetry direction $k^\parallel=0$, most of the d bands have a symmetry different from the s,p band. For example, all the d-band structures seen in the spectra of Figs. 2(a)–2(f) (spin arrows) have Δ_5 symmetry and do not interact with the s,p bands. Only the Δ_1 d band hybridizes with the s,p band. It gives rise to the spin polarization of thin-film states, as discussed in Sec. IV.

B. Preparation of atomically smooth films

In order to see clear, discrete thin-film states, we found it necessary to take great care with preparing smooth surfaces. Noble-metal substrates required electrochemical polishing to remove the damage from mechanical polishing. Otherwise, extensive sputtering was needed to remove the damage layer such that the sputter damage could not be healed completely by annealing. Likewise, after a series of thin-film depositions, such as those in Figs. 2(a) and 2(b), the sample went again through the complete polishing cycle, instead of sputtering off the overlayers. Detailed accounts of the surface preparation can be found elsewhere (Refs. 1 and 36 for noble metals,

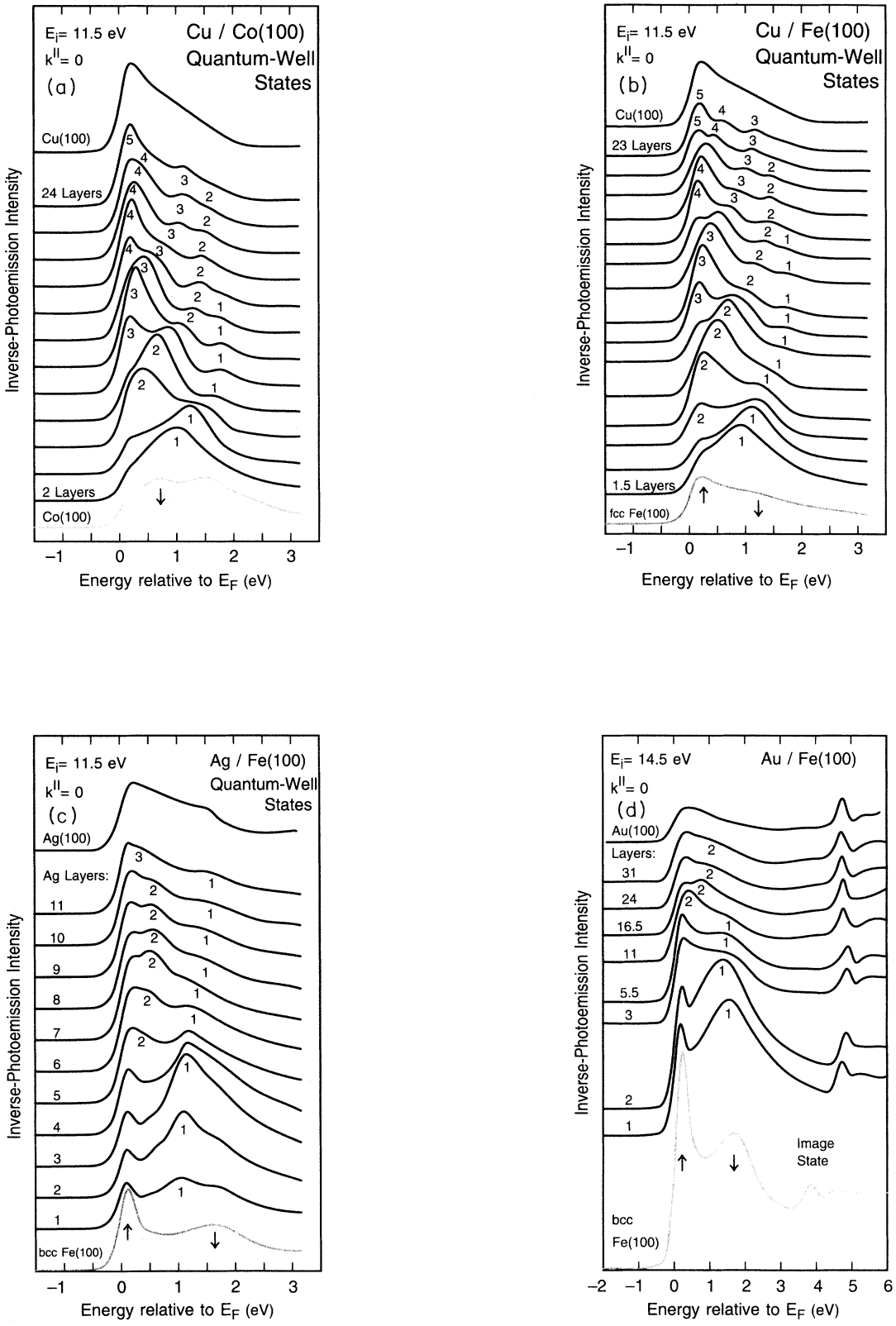

FIG. 2. Thickness dependence of inverse photoemission (a)–(f) and photoemission (g) and (h) from noble metals on ferromagnets, and vice versa ($k^{\parallel}=0$). The s,p band is split up into the numbered quantum-well states due to discretization of $k^{\perp}$ in a thin film (see Fig. 1). The thickness values are the same as for the structure plots in Figs. 3(a)–3(d).

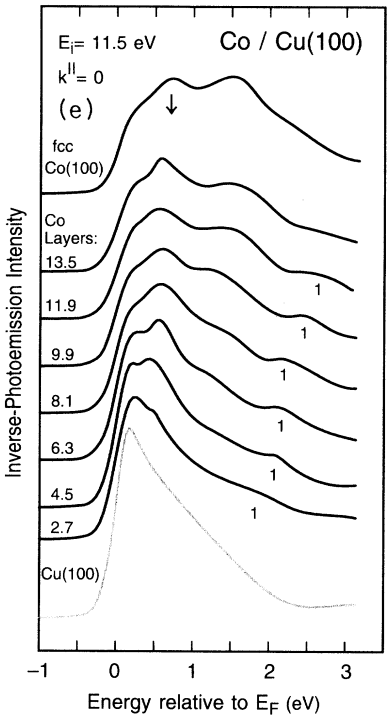

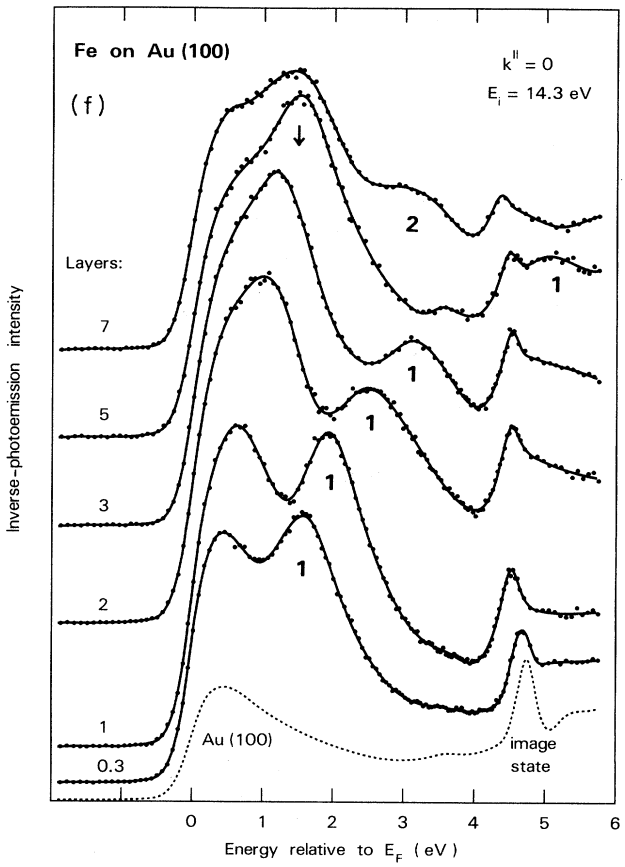

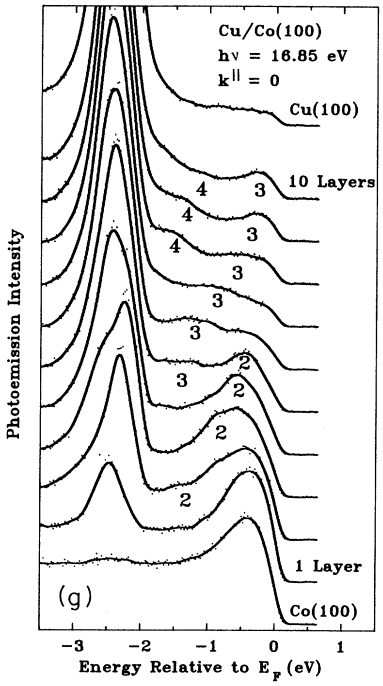

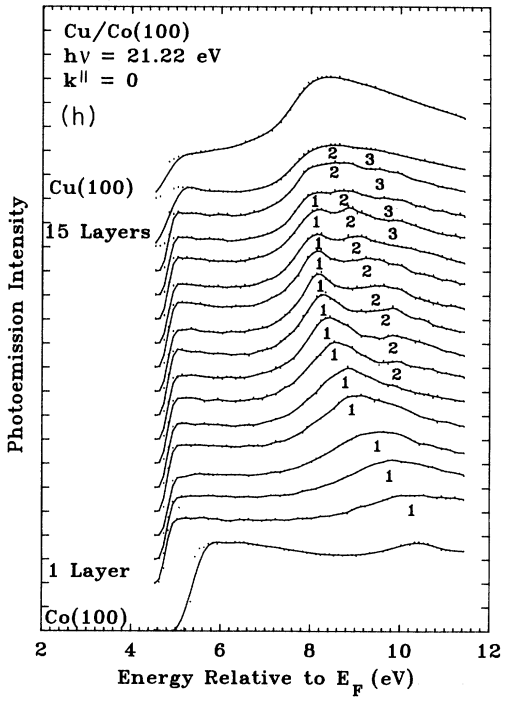

FIG. 2. (*Continued*).

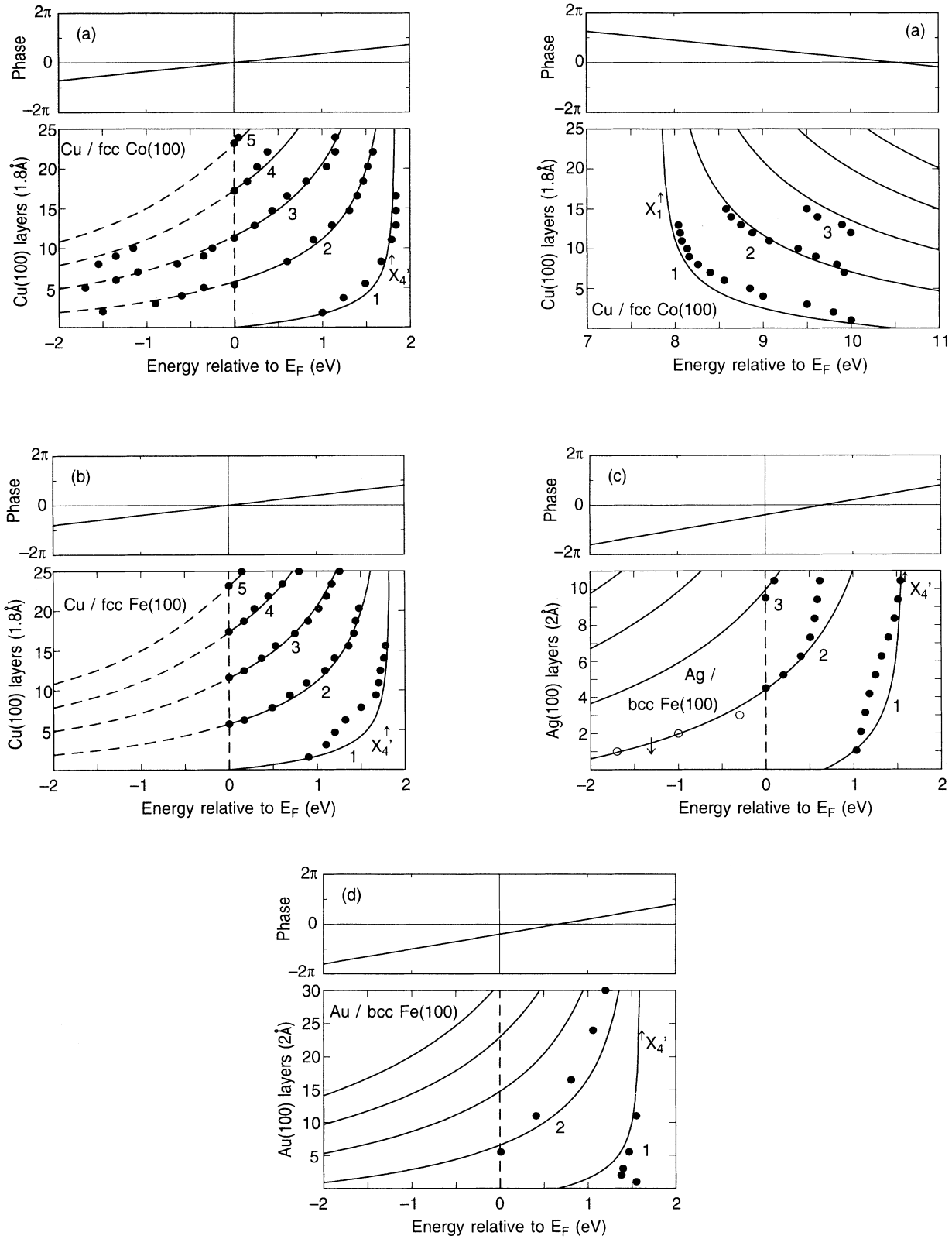

FIG. 3. Structure plots corresponding to data from Fig. 2 showing quantum-well states converging at large thicknesses toward the edges X_4' and X_1 of the s,p band. These states cross the Fermi level at regular thickness intervals (see Fig. 5). The lines are predictions from the bulk-band structures in Fig. 6, using the phase shifts shown in the top panels. Open circles in (c) are minority-spin states seen in photoemission (Ref. 33).

Ref. 38 for Fe). All overlayers were prepared by evaporation at pressures in the 10^{-10}-Torr regime with the sample held at room temperature to minimize interdiffusion. In some cases, annealing up to 150 °C gave somewhat sharper structures, e.g., for Co/Cu(100). We characterized the surfaces with low-energy electron diffraction and with inverse photoemission from image-potential surface states (compare Refs. 36–38). The most critical test for surface quality, however, was the existence and sharpness of discrete thin-film features in the (inverse) photoemission spectra. This is not surprising when looking at the strong film-thickness dependence of the spectra. For example, the Fe on Au(100) spectra in Fig. 2(f) show a maximum turning into a minimum when going from one- to two-layer coverage. Any roughness of as little as a single layer would therefore tend to smear the spectra into a structureless continuum. A smooth growth of ferromagnets on noble metals is particularly difficult, since the high surface energy of transition metals provides a strong driving force for clustering. In the case of Fe on Au(100), we believe the smooth morphology to be due to a monolayer of Au floating on top of the growing Fe film and playing the role of a surfactant (see Ref. 1).

III. WAVE FUNCTION OF THIN-FILM STATES

The framework for discussing thin-film states has been set by extensive work on quantum-well states in semiconductors (for a review see Ref. 39). As shown in Fig. 4, the wave function of a quantum-well state consists of a rapidly oscillating Bloch function, which is modulated by an envelope function. The Bloch function is derived from the bulk states at the nearest band edge, the envelope function ensures that the boundary conditions are met at the interfaces. This type of wave function originates from an expansion of the quantum-well wave function around the bulk wave functions of the nearest band edges. Often, a single band edge is sufficient [such as in Cu(100) at $k^{\parallel}=0$], but there exist cases with multiple band edges nearby [such as in Cu(100) at large $k^{\parallel}$; see Sec. IV B]. In all the spectra shown here, we have a single band edge, located at the Brillouin-zone boundary along the [100] direction (X for the fcc and H for the bcc lattice; see Fig. 1). In the case of a single band edge the modulation of the Bloch wave with wave vector k_{edge} by the envelope with wave vector k_{env} produces[40] a total wave vector

$$k_{\text{tot}}=k_{\text{edge}}\pm k_{\text{env}} \ . \tag{1}$$

It is understood that we only have to consider the components of these wave vectors perpendicular to the interface since the boundary conditions parallel to the interface are the same as in the bulk.

The total wave vector has to follow the dispersion of a bulk band as long as the quantum well is wide enough to neglect changes in the bonding near the interfaces. Basically, one assumes a bulk Hamiltonian and changes only the boundary conditions to those of a finite slab. Deviations from this behavior in films approaching the monolayer regime will be discussed in Sec. III C.

Outside the quantum well, the wave function decays with an exponential envelope into the substrate. There are no propagating states of the same symmetry at the same energy and $k^{\parallel}$ in a truly confined quantum-well state [e.g., for Δ_1 minority spin states in Ag on bcc Fe(100)]. The evanescent wave in the substrate corresponds to a band-gap solution with an imaginary part of the momentum perpendicular to the interface. Its decay constant is proportional to the square root of the energy distance from the band edge of the substrate. Thus, a large band offset between the band edges of the substrate and the confined layer gives rise to sharply confined wave functions. Compared to semiconductors with typically a few tenths of an eV band offset, one observes offsets of up to 9 eV in these metal systems,[1] giving rise to a confinement on an atomic scale. Even in films that do not exhibit strict confinement of the wave function, a strong resonance may build up in the film if the electron reflectivity at the boundary is high. We find such states in Cu on fcc Co(100) and Fe(100) and observe a behavior similar to true quantum-well states (see Sec. II A). Therefore, we will loosely call any thin-film state that fits this description a quantum-well state.

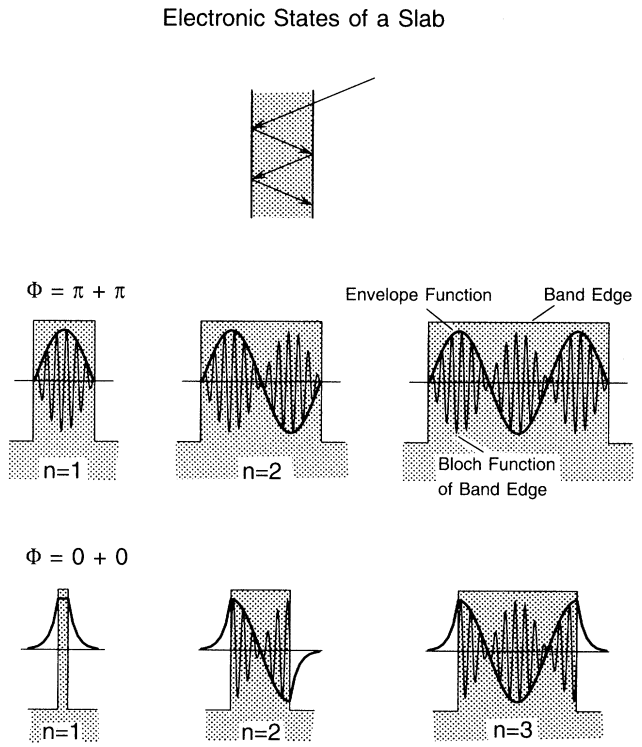

FIG. 4. Model wave functions of quantum-well states, and their explanation by a simple interferometer model. The fast-oscillating Bloch function at the band edge is modulated by a slowly varying envelope function. The latter ensures the proper boundary conditions, given by the phase shift ϕ at the two interfaces. The wave functions are confined to the shaded regions in the energy-vs-z diagrams, where bulk bands exist.

A. Measuring the wavelength of the envelope

We wish to determine how we can measure the characteristic quantum numbers of a quantum-well state. Since it is easy to figure out the k vector of the band edge from the bulk-band topology, the problem boils down to measuring the k vector of the evelope function $k_{\rm env}$. For this purpose we use a method that determines the wavelength of the envelope function directly (see Ref. 1). It can be explained by a simple interferometer model, as shown in Fig. 4 (top). The interfaces confining the quantum well are analogous to the mirrors of a Fabry-Perot interferometer. True quantum-well states are produced by 100% reflectivity, and resonances by partial reflectivity. By varying the spacing of the interferometer mirrors one obtains interference fringes with a periodicity of half the wavelength of the light, due to the double pass per round trip. Likewise, we expect interference fringes in the electron wave function to appear with a period p of half the wavelength $\lambda_{\rm env}$ of the envelope function when changing the thickness of the quantum well (compare Fig. 4, middle):

$$p=\lambda_{\rm env}/2 \ . \tag{2a}$$

Thus, one obtains $k_{\rm env}=2\pi/\lambda_{\rm env}$ from the period p:

$$k_{\rm env}=\pi/p \ . \tag{2b}$$

Such regularly spaced interference fringes are indeed observed, as shown in Figs. 5(a)–5(c). A key ingredient of this method for determining $k_{\rm env}$ is changing the thickness while keeping the energy of the electrons fixed[1] (initial- as well as final-state energy). Therefore, one eliminates the energy-dependent phase shifts for the two interface reflections, which would have to be included if we were to analyze peak positions for a (inverse) photoemission spectrum (see Secs. III B and IV C). Previous measurements[28–32] of quantum-well states varied the electron energy at fixed thickness and had to deal with these phase shifts. Although phase shifts can be estimated using model potential barriers,[41,42] it is always preferable to avoid any model dependence for the analysis.

There is very little damping in the intensity oscillations at the Fermi level up to a critical point [about 20 layers for Cu on fcc Co(100) and fcc Fe(100), 12 layers for Ag on bcc Fe(100), and eight layers for Fe on Au(100)]. This is consistent with the long mean free path of electrons near the Fermi level. There are two possible reasons for the sudden quenching of the oscillations. One is degrading film quality, e.g., due to the depletion of the Au surfactant layer for Fe on Au(100) or to the accumulated amount of impurities from a long sequence of evaporations. The other possible cause is our finite energy resolution, which makes it harder to separate adjacent quantum-well states when their spacing becomes smaller in thick films.

B. Obtaining the bulk-band structure from thin-film states

For thick films, it is possible to obtain accurate bulk-band-structure information from quantum-well states as pointed out previously.[29–32,43] Such results are given in Fig. 6 for our data. In our picture, we only have to determine the wave vector $k_{\rm env}$ of the envelope function from the period p of intensity oscillations using Eq. 2(b). Then we can use Eq. (1) to determine the total wave vector $k_{\rm tot}=k$ of the bulk band. The band-edge wave vector $k_{\rm edge}$ in Eq. (1) corresponds to the zone-boundary wave vector $k_{\rm ZB}$ at X or H for the data shown here, i.e., with electrons incident or emitted normal to the [100] face of fcc or bcc metals. Using $k_{\rm ZB}=\pi/d$, where d is the layer spacing, we arrive at a simple relation between the period p and the band wave vector k,

$$k=1-1/p \ , \tag{3a}$$

$$p=1/(1-k) \ , \tag{3b}$$

with k in units of $k_{\rm ZB}$ and p in monolayers. This method of using quantum-well states to determine three-dimensional band dispersions provides an absolute measurement that does not depend on modeling the upper-state band in the (inverse) photoemission experiments. The present limitation of its accuracy is surprisingly not fundamental, but due to the uncertainties in the thickness determination of the evaporated films. Despite monitoring the rate with a quartz microbalance and additional calibrations by Rutherford backscattering, small-angle x-ray diffraction, and reflection high-energy electron diffraction oscillations we estimate an uncertainty of about $\pm 10\%$. The best cross check turns out to be the Fermi wave vector from de Haas-van Alphen data.[44] Apart from this technical problem we have to consider a limitation of the method due to changes in the bonding for interface atoms. We will look into this question in Sec. III C and find that the contribution from interface atoms becomes significant at a thickness of about 5 layers.

For the noble metals, we obtain the full dispersion of s,p bands near the X point by fitting a simple band model[41,42] to the available data (see lines in Fig. 6 and Table I for the relevant band parameters). The model uses the effective mass m^*, the average inner potential V_0, and the lowest Fourier component of the potential along the [100] direction as parameters. The latter equals half the X_4'-X_1 band gap. These three parameters are matched to the Fermi level crossing k_F obtained from de Haas-van Alphen data,[44] the transition energy to the upper branch of the s,p band at k_F (see Refs. 36, 45, and 46), and the X_4' point determined from the asymptotic energy of the first quantum-well state for large film thickness [Figs. 3(a)–3(d)]. The resulting critical points can be compared with independent measurements[30,36,37,45] that use the intensity dropoff at the band edges as markers for X_4' and X_1 (see footnotes to Table I).

The energies of quantum-well states can be modeled by our empirical bulk bands if we include energy-dependent phase shifts [top of Figs. 3(a)–3(d)]. The formula for the thickness-versus-energy relation of the nth quantum-well state, $d_n(E)$, is obtained by adding $(n-1)$ times the period p [from Eq. 3(b)] to the thickness for the first state, which is given by a fraction ϕ of the period, with ϕ being the sum of the phase shifts for the reflections at the two interfaces, measured in units of 2π:

$$d_n(E)=[n-1+\phi(E)]/[1-k(E)]\ . \quad (4)$$

d_n is given in monolayers, and k in units of the zone-boundary wave vector k_{ZB} at X. For the noble metals, we use the empirical band structures $k(E)$ shown in Fig. 6 and a linear expansion of the phase shifts $\phi(E)$. The phase shifts are found by matching the calculated structure plots [lines in Figs. 3(a)–3(d)] to the data for one of the quantum-well states. The results are qualitatively similar to those obtained from the energies of image states and s,p-like surface state.[41,42] $\phi(E)$ increases with energy near the Fermi level since the classical turning point on the vacuum side moves out with increasing energy, following a truncated image potential. On the substrate side only a small phase shift is expected, since the energy of the quantum-well states is close to the X_4' point, where the phase shift is zero (see Sec. IV C). The calculated positions of quantum-well states in Figs. 3(a)–3(d)

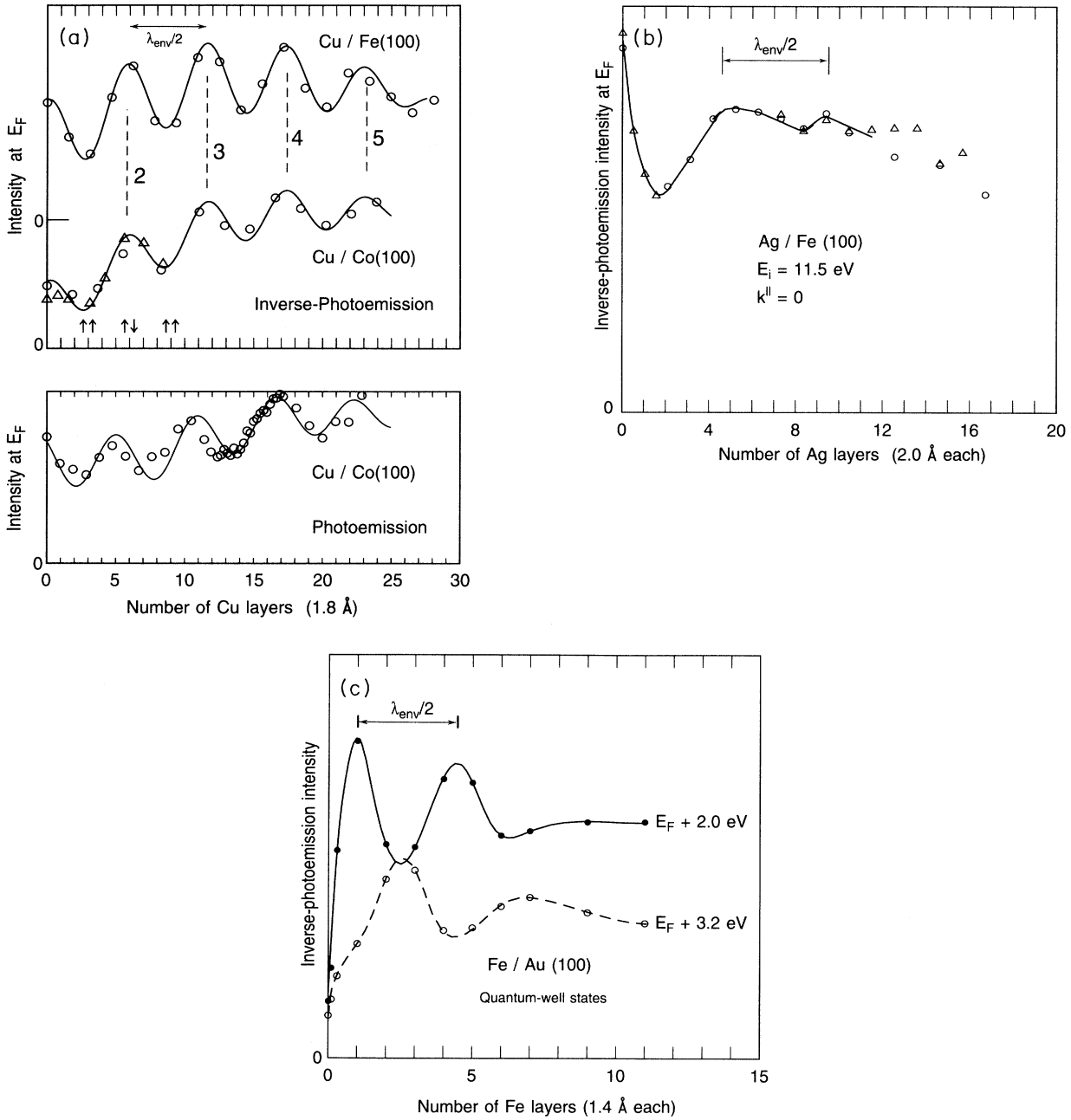

FIG. 5. Oscillations in the inverse photoemission intensity vs film thickness. They can be understood as interference fringes appearing with a periodicity of half the wavelength of the envelope function λ_{env} (see Fig. 4). Maxima appear when quantum-well states cross the Fermi level (see Fig. 2). The oscillation period of six layers is equal to the magnetic-oscillation period observed[6,7] for Co/Cu(100) superlattices (spin arrows).

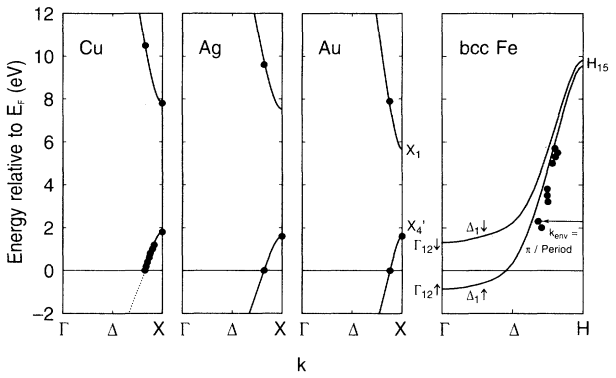

FIG. 6. Band structure of the s,p bands with Δ_1 symmetry obtained from quantum-well states. The wave vector k equals the wave vector k_{edge} at the band edge (X_4' or H_{15}) minus the wave vector of the envelope function k_{env}, which is obtained from the period of intensity oscillations (Fig. 5). The s,p bands of fcc Fe(100) and Co(100) are similar to those of Cu(100) with an upwards shift (Ref. 37) of 1–2 eV.

fit the data reasonably well. Deviations for thick films of Ag and Au are probably due to degrading film quality, which shows up as a weakening of the quantum-well features in Figs. 2(c) and 2(d). At about five-layer film thicknesses there are systematic deviations for the $n=1$ state, which will be discussed in Sec. III C. In order to get the best fit for the photoemission data in Cu we had to modify the simple, one-Fourier-component s,p-band structure below E_F to account for hybridization with the Cu d-band [dashed lines in Figs. 3(a) and 6].

For Cu/Co(100) we observe quantum-well states at both edges of the s,p band gap, i.e., X_4' and X_1. The states near X_1 are seen as a modulation in the intensity of secondary electrons transmitted through the Cu overlayer [Fig. 3(a), right-hand side]. Such states have shown up in previous work[30] as a modulation of the sample current with energy under a low-energy electron beam.

TABLE I. Band-structure parameters of noble metals along [100] relevant for quantum-well states. v_F is the Fermi velocity, E_{up} the energy of the upper branch of the s,p band.

	k_F ($2\pi/a$)	v_F (10^6 m/sec)	X_4' (eV)	X_1 (eV)	$E_{up}(k_F)$ (eV)	V_0-E_F (eV)	m^* (m_e)
Cu	0.827[a]	1.2	1.8[b]	7.8[c]	10.5[d]	−6.9	0.88[e]
Ag	0.819[a]	1.4	1.6[b]	7.5[c]	9.6[d]	−7.2	1.18[e]
Au	0.878[a]	1.2	1.6[b]	5.7[c]	7.9[f]	−7.7	0.74[e]

[a]From de Haas–van Alphen data, Ref. 44.

[b]Values of X_4' obtained from the asymptotic behavior of the $n=1$ quantum-well state at large thicknesses. There exist upper limits for X_4' from the inflection point of the intensity dropoff in inverse photoemission (Ref. 36): 1.8 eV for Cu, 1.9 eV for Ag, and 2.3 eV for Au.

[c]Values of X_1 obtained from fitting the empirical band-structure described in the text to k_F, X_4', and $E_{up}(k_F)$. The corresponding value from the inflection point of the intensity dropoff of secondary electrons is 7.8 eV for Cu (Ref. 36). Compare also the value of 7.9 eV in Ref. 45, and the inflection point of the sample current at 7.3 eV in Ref. 30.

[d]From inverse photoemission (Ref. 36) and photoemission (Ref. 45). Note that Ref. 45 gives a transition energy of 10.6 eV at an initial energy 0.13 eV below E_F for Cu, which moves down to 10.5 eV for an initial state at E_F (see Ref. 36).

[e]This effective-mass parameter corresponds to the kinetic-energy term in our three-parameter band model. Its physical significance may be blurred by the fact that it partially simulates the effect of neglected Fourier components of the potential. The uncertainty of the fit is ±10%.

[f]From inverse photoemission (Ref. 36) and photoemission (Ref. 46).

C. Towards the monolayer limit: Bonding across the interface

The simple picture of quantum-well states as bulk states, discretized by the finite slab thickness, is expected to break down when going toward the monolayer limit. The atoms in the quantum well will feel their foreign neighbors across the interface and will change their bulklike bonding. The onset of this effect can be observed by comparing our data with the predictions of the bulklike quantum-well model in the low-thickness limit. Looking at the structure plots for noble-metal overlayers in Figs. 3(a)–3(d), we notice that the $n=1$ quantum-well state deviates systemically from the energy predicted by the bulklike quantum-well model (lines). This change proceeds in two phases. At about five layers the $n=1$ state moves away from the band edge faster than predicted. Then, in the monolayer limit, this trend is reversed, and the movement of the $n=1$ state stalls, or even reverses its direction.

There are some changes in the magnetic behavior of thin films that happen in the same thickness regime where we observe deviations from bulklike bonding in quantum wells. Critical exponents in magnetic overlayers change from three-dimensional to two-dimensional behavior between seven and five layers.[47] Also, the Curie temperature becomes reduced in thin films. It comes down to half the bulk value at a thickness between four and five layers.[48]

When considering the bonding across interfaces we have to know how far the quantum-well wave functions extend into the classically forbidden region outside the well. One expects an exponentially decaying envelope function in this region with an imaginary wave vector corresponding to the square root of the well depth, or band offset. For two metals with identical lattices this band offset is about 1 or 2 eV, as seen here for fcc Cu versus fcc Co and Fe and in previous work[28–32] for fcc metals. Such an offset provides decay constants of several atomic layers. When growing a bcc structure on lattice-matched fcc substrate, such as for Fe on Au(100), the band offset can be as large as 9 eV between X_4' and H_{15}, due to the different band topologies (see Fig. 6 and Ref. 49 for the band structure of Fe; the experimental H_{15} point is at 10.2 eV). This offset is an order of magnitude larger than in any quantum well studied to date, and provides a decay constant of atomic dimensions. Thus, we have come a step closer to the ultimate goal of manipulating materials layer by layer, not only in their structure but also concerning their wave functions.

IV. IMPLICATIONS FOR OSCILLATORY MAGNETIC COUPLING

An oscillatory magnetic coupling has been observed in superlattices consisting of alternating layers of ferromagnets and noble metals.[5–16] This effect has potential for applications in magnetic storage since it causes a large ("giant") decrease in the resistivity when the alignment is switched from antiferromagnetic to ferromagnetic by an external field. The change in resistivity can be used to read information stored on magnetic disks. Special spin-valve structures[18] have been designed for this purpose. Our thin-film studies can serve as model for more complex structures by representing one period of a superlattice or a spin valve. A single layer is expected to simulate a superlattice rather well, since the observed magnetic coupling depends mainly on the noble-metal spacer layers, and little on the thickness of the ferromagnetic layers. Therefore, expanding a thin magnetic film to an infinitely thick ferromagnetic substrate does not change the magnetic couplings.

As we have pointed out in the preceding sections, the quantization of $k^{\perp}$ is a general characteristic of thin-film structures, and thus should influence their magnetic behavior as well. Looking for electronic states that are responsible for magnetic coupling, we have to focus on states within about $k_B T_C$ of the Fermi level (T_C is the Curie or Neel temperature, k_B is the Boltzmann constant), since the rearrangement of these states drives the phase transition, similarly to the opening of a gap around the Fermi level driving the superconductivity phase transition. For magnetotransport states within about $k_B T_a$ are relevant (T_a being the ambient temperature). There are several strong indications that the quantum-well states observed at the Fermi level in thin noble-metal films are, in fact, the carriers of the magnetic coupling: They appear with a period equal to the magnetic period in cases where a comparison can be made, e.g., for fcc Cu/Co(100). They also can be spin polarized despite their s,p character, thus providing a magnetic interaction. Other noteworthy consistency checks come from the prediction that the magnetic-coupling period should depend only on the noble-metal spacer, not on the ferromagnetic substrate, while the phase depends only on the substrate. In the following, we will explain these phenomena using the quantum-well-state picture developed in Sec. III A. It turns out that the result for the periodicity of the magnetic coupling is identical to that obtained from RKKY theory when evaluated at discrete lattice spacings. Thus, we have found a real-space picture that should make the workings of the RKKY formalism more tractable.

A. Spin polarization of s,p states in noble metals

First we focus on the spin polarization of quantum-well states. As an example, we discuss fcc Ag(100) on bcc Fe(100), which is a system that has been studied with spin-polarized photoemission.[33] An occupied minority-spin state has been found at $k^{\parallel}=0$ [open circles in Fig. 3(c)], that connects with our $n=2$ quantum-well state through the Fermi level. Thus, we have good reason to believe that the quantum-well state has minority-spin character as well. This can be explained from the band structure[49] for Ag(100) and Fe(100) in Fig. 6. The minority-spin Δ_1 bands exhibit a gap at E_F in Fe(100), allowing the formation of true quantum-well states in the minority Δ_1 s,p band of Ag(100). The majority-spin Δ_1 states of Ag(100), on the other hand, couple to the majority Δ_1 band of Fe(100) at the Fermi level and form a continuum of Bloch states, instead of discrete quantum-well states.

In order to get an idea of the spin distribution in the Ag(100) layer, we model the charge and spin densities in Fig. 7 by simple, sinusoidal-model wave functions. The charge density of the minority-spin quantum-well state is modulated with half the wavelength of the envelope function, the factor $\frac{1}{2}$ originating from squaring the wave function. In addition, there are fast oscillations present in both the Bloch and the quantum-well states. The combined spin density of these two states is obtained by subtracting their charge densities. The result retains the long periodicity $\lambda_{\mathrm{env}}/2$ from the quantum-well state. The same period shows up when the spin density is evaluated at discrete lattice spacings (dots in Fig. 7). Note, though, that Fig. 7 represents a snapshot of the spin distribution at a fixed thickness, i.e., what one would see if one could look into the Ag film. In magnetic-oscillation experiments, one varies the film thickness, causing the minority-spin density of the quantum-well state to appear and disappear periodically (as in Fig. 5), while the majority-spin Bloch state remains nearly unaffected. Therefore, one obtains a periodic change in the spin density exhibiting again the $\lambda_{\mathrm{env}}/2$ period, except that the factor $\frac{1}{2}$ comes in this case from the interferometer effect shown in Fig. 4. So far, we have considered the spin distribution at a specific energy $E=E_F$ and $k^{\parallel}=0$. For the

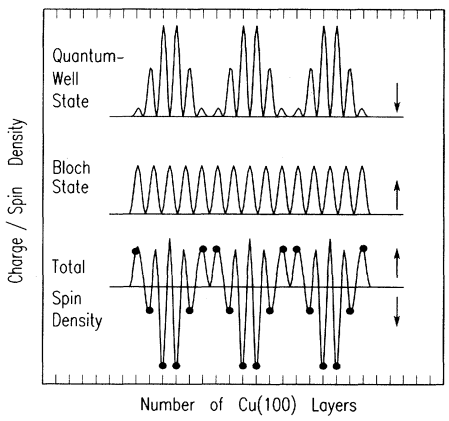

FIG. 7. Charge and spin densities for states at the Fermi level in Ag on Fe(100). Due to the boundary conditions at the interface, only a minority-spin quantum-well state can exist, while the majority spins in Ag(100) couple to the majority-spin Δ_1 band of Fe(100) (Fig. 6). Subtracting the minority-spin density of the quantum-well state (top) from the majority-spin density of the Bloch state (middle) produces an oscillatory total-spin density (bottom) in the Ag(100) film that can transmit magnetic coupling.

total spin density one would have to integrate over E and $k^{\parallel}$ (compare Sec. IV B).

The spin-polarization of s,p-like quantum-well states should also be seen in other magnetic measurements. Indeed, there are indications that for the system Fe/Au(100) the Fe s,p quantum-well states show up in magneto-optical measurements.[50] The energy of extra transitions seen for Fe films thinner than 10 Å and their thickness dependence are very similar to the behavior of the $n=1$ quantum-well state in Fig. 2(f) and Ref. 1.

B. Oscillation period

The periodicity in the appearance of quantum-well states at E_F can be traced directly to the Fermi wave vector k_F by using Eq. (3b). The de Haas-van Alphen Fermi wave vectors[44] of 0.827, 0.819, and 0.878 (in units of k_{zb}) for the [100] direction in Cu, Ag, and Au give rise to periods of $1/(1-0.827)=5.8$ layers for Cu(100), $1/(1-0.819)=5.5$ layers for Ag(100), and $1/(1-0.878)=8.2$ layers for Au(100). These agree with our measured quantum-well-state periods of 5.9 layers for Cu/Co(100) and five layers for Ag/Fe(100) within the experimental accuracy. The magnetic-oscillations periods reported for Cu/Co(100) fall into the same range (6 layers[6] and 5.5 layers;[7] in Ref. 9, two periods of 8.0 and 2.6 layers have been obtained by modeling, but the spacing of the main maxima is about the same as in Refs. 6 and 7, corresponding to the difference between the two periods, i.e., 5.4 layers). For Ag/Fe(100) a magnetic period of 4–5 layers has been found recently in very smooth films,[10] which is comparable to the quantum-well-state period. For Au/Fe(100) a long period of 6.9 layers has been found,[16] together with an antiferromagnetic two-layer period.

The same result for the periodicity has come up in theoretical treatments of the exchange coupling in superlattices,[19–23] where the RKKY coupling is evaluated at discrete lattice spacings. By coupling the RKKY wave vector $2k_F$ with a reciprocal-lattice vector $g=2k_{ZB}$ one obtains an oscillation wave vector $2(k_{ZB}-k_F)$ which is identical to the wave vector $2k_{env}=2(k_{edge}-k_F)$ resulting from the periodicity in the appearance of quantum-well states at the Fermi level with varying film thickness [Eqs. (1) and (2); note that the band edge is located at the zone boundary].

So far, we have considered the contribution of quantum-well states at a parallel wave vector $k^{\parallel}=0$. They might be expected to dominate the magnetic coupling by symmetry. In order to see the effect of other $k^{\parallel}$ on the period, we analyze the situation for the high-symmetry planes of Cu(100) and Cu(111) in Fig. 8. The arrows represent the wave vectors k_{env} of envelope functions at various $k^{\parallel}$, extending from various edges of the s,p band (dotted lines) to the Fermi surface. Their length is inversely proportional to the quantum-well-state period. For Cu(100), the value of k_{env} at $k^{\parallel}=0$ turns out to be representative of large portions of the Fermi surface. This explains why the period at $k^{\parallel}=0$ worked so well for explaining magnetic oscillations. According to RKKY theory,[22] there exists an additional, shorter

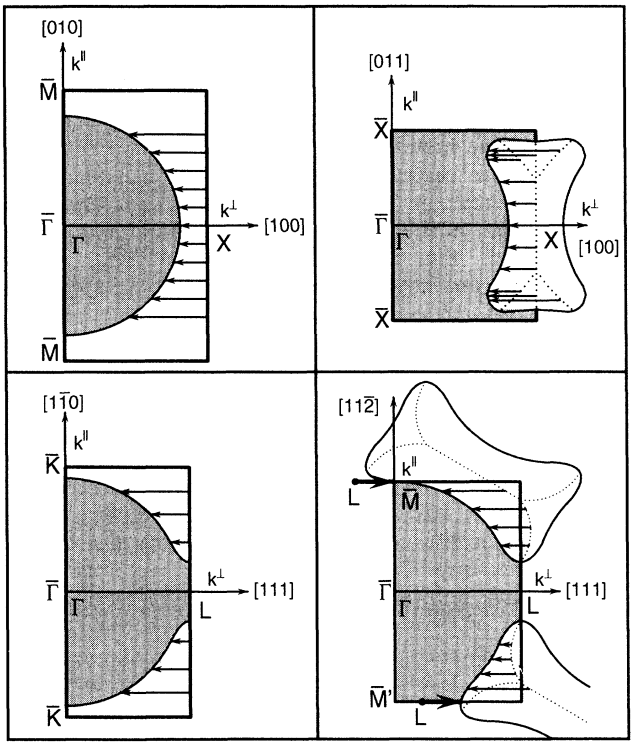

FIG. 8. Summation over oscillation periods for quantum-well states at the Fermi level in Cu(100) and Cu(111) films (top and bottom, respectively). The arrows represent the wave vectors of the envelope wave functions that determine the magnetic coupling period. They point from s,p band edges (dotted lines) to the Fermi surface. For Cu(100), the period near $k^{\parallel}=0$ dominates, whereas for Cu(111) there are no quantum-well states at $k^{\parallel}=0$ and a variety of periods at other $k^{\parallel}$.

period due to states near the end of the "dog bone"-shaped Fermi surface, i.e., at large $k^{\parallel}$. Recent observations do, indeed, find additional, short periods of 2.6 layers[9] in Cu/Co(100), and 2.0 layers[16] in Au/Fe(100). The analogy between RKKY theory and our quantum-well-state model is less obvious in this case, since RKKY predicts a single period corresponding to $2(k_{ZB}-k_F)$, whereas the quantum-well-state model predicts states made up of wave functions from three nearby band extrema, i.e., a minimum at the zone boundary and two maxima symmetric to it. Their average k is symmetric to the zone boundary, however, and, thus, equivalent to the RKKY result. RKKY, as well as the quantum-well model, predict that the short period should originate from states with $k^{\parallel}$ near the end of the dog bone, and not at $k^{\parallel}=0$, where all the existing spectroscopic data have been taken.

Cu(111) is a more complicated case than Cu(100). There are no quantum-well states at the Fermi level for $k^{\parallel}=0$, since the Fermi level lies in the s,p band gap along the [111] direction. Going to finite $k^{\parallel}$ one does encounter quantum-well states at E_F, but their periods vary over a wide range. That can be seen already for the fraction of all possible k_{env} that is shown in Fig. 8 or Cu(111). When averaging over all $k^{\parallel}$, the different periods largely com-

pensate each other. This may be the explanation for the difficulties in coming to an agreement on the existence of intrinsic magnetic oscillations in Cu/Co(111) superlattices.[4,8,14,15] The principal periodicity remaining after the $k^{\parallel}$ average in RKKY theory[22] can be assigned to quantum-well states derived from the L minima at large $k^{\parallel}$ ($\bar{M}$ and $\bar{M}'$; see heavy arrows in Fig. 8). This analogy suggests again that the quantum-well and the RKKY picture are equivalent.

C. Oscillation phase

The phase of the quantum-well-state oscillations depends on the phase shifts encountered by the wave function as it is back reflected at the boundaries of the quantum well. It depends on the energy relative to the edges of the band gap that causes the reflection.[41,42,51] For the "inverted" s,p gap at the zone boundary in noble metals and transition metals, the phase shift ranges from 0 at the "antibonding," p_z-like bottom of the gap[51] (X_4' for fcc and H_{15} for bcc) to π at the "bonding," s-like top (X_1 for fcc and H_1 for bcc). For the s,d gap at the zone center, the situation is reversed. For example, the bonding, d_{z^2}-like Γ_{12} point in bcc Fe has a phase shift zero. Since the Fermi level is not too far away from the X_4' point in fcc metals and close to the Γ_{12} point in bcc metals, we may assume a phase shift of zero to a first approximation. As a consequence, the envelope function will develop maxima at the interfaces, as shown in Fig. 4, bottom. The $n=1$ state degenerates to a δ function in an infinitely thin quantum well. For Ag/Fe(100) this expectation agrees with a band calculation,[33] which lead to the previous interpretation of the occupied $n=2$ quantum-well state as interface state. On the vacuum side of a film, the phase shift is harder to estimate, since the Fermi level lies in the transition region between the Coulomblike image barrier near the vacuum level and the saturation of the image potential at the inner potential. Therefore, the phase seen for quantum-well states sandwiched between vacuum and ferromagnetic substrate in our experiments is generally not representative of the phase for a noble metal embedded in a ferromagnet, as in magnetic superlattices. Thus, while the period of quantum-well states depends only on the material in the well, the phase is determined exclusively by the material that confines the well. Magnetic oscillations in superlattices behave in a similar way. In the case of Cu/Co(100) versus Cu/Fe(100), identical periods have been reported, but a variety of phases.[8,9]

ACKNOWLEDGMENTS

We would like to acknowledge M. Kief for stimulating interactions in the early phase of this work, M. Copel for Rutherford-backscattering measurements, and E. Spiller for small-angle x-ray-diffraction measurements, which were used in the calibration of our film thickness.

[1]F. J. Himpsel, Phys. Rev. B **44**, 5966 (1991).
[2]J. E. Ortega and F. J. Himpsel, Phys. Rev. Lett. **69**, 844 (1992).
[3]M. N. Baibich, J. M. Broto, A. Fert, F. Nguyen Van Dau, F. Petroff, P. Etienne, G. Creuzet, A. Friederich, and J. Chazelas, Phys. Rev. Lett. **61**, 2472 (1988); A. Barthélemy, A. Fert, M. N. Baibich, S. Hadjoudj, F. Petroff, P. Etienne, R. Cabanel, S. Lequien, F. Nguyen Van Dau, and G. Cruezet, J. Appl. Phys. **67**, 5908 (1990).
[4]S. S. P. Parkin, N. More, and K. P. Roche, Phys. Rev. Lett. **64**, 2304 (1990); S. S. P. Parkin, R. Bhadra, and K. P. Roche, *ibid.* **66**, 2152 (1991); S. S. P. Parkin, R. F. Marks, R. F. C. Farrow, G. R. Harp, Q. H. Lam, and R. J. Savoy, Phys. Rev. B **46**, 9262 (1992).
[5]S. S. P. Parkin, Phys. Rev. Lett. **67**, 3598 (1991).
[6]J. J. de Miguel, A. Cebollada, J. M. Gallego, R. Miranda, C. M. Schneider, P. Schuster, and J. Kirschner, J. Magn. Magn. Mater. **93**, 1 (1991); A. Cebollada, R. Miranda, C. M. Schneider, P. Schuster, and J. Kirschner, *ibid.* **102**, 25 (1991).
[7]Z. Q. Qiu, J. Pearson, and S. D. Bader, Phys. Rev. B **46**, 8659 (1992).
[8]W. R. Bennett, W. Schwarzacher, and W. F. Egelhoff, Phys. Rev. Lett. **65**, 3169 (1990); F. Petroff, A. Barthélemy, D. H. Mosca, D. K. Lottis, A. Fert, P. A. Schroeder, W. P. Pratt, Jr., and R. Loloee, Phys. Rev. B **44**, 5355 (1991).
[9]M. T. Johnson, S. T. Purcell, N. W. E. McGee, R. Coehoorn, J. aan de Stegge, and V. Hoving, Phys. Rev. Lett. **68**, 2688 (1992); M. T. Johnson, R. Coehoorn, J. J. de Vries, N. W. E. McGee, J. aan de Stegge, and P. J. H. Bloemen, *ibid.* **69**, 969 (1992).
[10]Z. Celinski and B. Heinrich, J. Magn. Magn. Mater. **99**, L25 (1991); recently, a magnetic period of 4–5 layers has been seen in very smooth Ag films on bcc Fe(100): Z. Celinski, B. Heinrich, and J. F. Cochran, J. Appl. Phys. (to be published).
[11]M. E. Brubaker, C. H. Sowers, and S. D. Bader, Appl. Phys. Lett. **58**, 2306 (1991).
[12]J. Unguris, R. J. Celotta, and D. T. Pierce, Phys. Rev. Lett. **67**, 140 (1991).
[13]Qibiao Chen, M. Onellion, and A. Wall (unpublished).
[14]W. F. Egelhoff, Jr. and M. T. Kief, Phys. Rev. B **45**, 7795 (1992).
[15]D. Greig, M. J. Hall, C. Hammond, B. J. Hickey, H. P. Ho, M. A. Howson, M. J. Walker, N. Wiser, and D. G. Wright, J. Magn. Magn. Mater. **110**, L239 (1992).
[16]A. Fuss, S. Demokritov, P. Grünberg, and W. Zinn, J. Magn. Magn. Mater. **103**, L221 (1992).
[17]P. Grünberg, R. Schreiber, Y. Pang, M. B. Brodsky, and H. Sowers, Phys. Rev. Lett. **57**, 2442 (1986); G. Binasch, P. Grünberg, F. Saurenbach, and W. Zinn, Phys. Rev. B **39**, 4828 (1989).
[18]B. Dieny, V. S. Speriosu, S. S. P. Parkin, B. A. Gurney, D. R. Wilhoit, and D. Mauri, Phys. Rev. B **43**, 1297 (1991); B. Dieny, V. S. Speriosu, S. Metin, S. S. P. Parkin, B. A. Gurney, P. Baumhart, and D. R. Wilhoit, J. Appl. Phys. **69**, 4774 (1991).
[19]D. M. Edwards, J. Mathon, R. B. Muniz, and M. S. Phan, Phys. Rev. Lett. **67**, 493 (1991).
[20]D. M. Deaven, D. S. Rokhsar, and M. Johnson, Phys. Rev. B **44**, 5977 (1991).
[21]F. Herman, J. Sticht, and M. Van Schilfgaarde, J. Appl. Phys. **69**, 4783 (1991); F. Herman and R. Schrieffer, Phys. Rev. B

46, 5806 (1992); F. Herman, M. Van Schilfgarde, and J. Sticht, *Proceedings of the International Conference on the Physics of Transition Metals, Darmstadt 1992* [Int. J. Mod. Phys. (to be published)].

[22]C. Chappert and J. P. Renard, Europhys. Lett. **15**, 553 (1991); P. Bruno and C. Chappert, Phys. Rev. Lett. **67**, 1602 (1991); **67**, 2592 (1991) (the latter shows the origin of various periodicities in k space); Phys. Rev. B **46**, 261 (1992).

[23]R. Coehoorn, Phys. Rev. B **44**, 9331 (1991).

[24]Y. Yang, P. M. Levy, and J. L. Fry, Phys. Rev. Lett. **65**, 2732 (1990); J. L. Fry, E. C. Ethridge, P. M. Levy, and Y. Wang, J. Appl. Phys. **69**, 4780 (1991).

[25]K. B. Hathaway and J. R. Cullen, J. Magn. Magn. Mater. **104-107**, 1840 (1992); J. C. Slonczewski, Phys. Rev. Lett. **67**, 3172 (1991); B. A. Jones and C. Hanna (unpublished); Vadim Kalmeyer (unpublished).

[26]H. Erschbaumer, A. J. Freeman, C. L. Fu, and R. Podloucky, Surf. Sci. **243**, 317 (1991); In Fig. 1 this calculation has been shifted up by 0.5 eV to match the X_4' point of the bulk calculations (Ref. 27). For a Cu(100) slab calculation, see J. G. Gay, J. R. Smith, and F. J. Arlinghaus, Phys. Rev. Lett. **42**, 332 (1979).

[27]H. Eckhardt, L. Fritsche, and J. Noffke, J. Phys. F **14**, 97 (1984).

[28]R. E. Thomas, J. Appl. Phys. **41**, 5330 (1970).

[29]R. C. Jaklevic, J. Lambe, M. Mikkor, and W. C. Vassell, Phys. Rev. Lett. **26**, 88 (1971); R. C. Jaklevic and John Lambe, Phys. Rev. B **12**, 4146 (1975); H. Hammer, W. Hartweck, D. Stark, and P. Zwicknagl, Appl. Phys. **11**, 41 (1976); M. Jalochowski, E. Bauer, H. Knoppe, and G. Lilienkamp, Phys. Rev. B **45**, 13607 (1992).

[30]Hiroshi Iwasaki, B. T. Jonker, and Robert L. Park, Phys. Rev. B **32**, 643 (1985).

[31]S. Å Lindgren and L. Walldén, Phys. Rev. Lett. **61**, 2894 (1988).

[32]T. Miller, A Samsavar, G. E. Franklin, and T. -C. Chiang, Phys. Rev. Lett. **61**, 1404 (1988); M. A. Mueller, A. Samsavar, T. Miller, and T. -C. Chiang, Phys. Rev. B **40**, 5845 (1989); M. A. Mueller, T. Miller, and T. -C. Chiang, *ibid.* **41**, 5214 (1990).

[33]N. B. Brookes, Y. Chang, and P. D. Johnson, Phys. Rev. Lett **67**, 354 (1991).

[34]D.Kerkmann, D. Pescia, J. W. Krewer, and E. Vescovo, Z. Phys. B **85**, 311 (1991).

[35]M. Jalochowski, H. Knoppe, G. Lilienkamp, and E. Bauer, Phys. Rev. B **46**, 4693 (1992).

[36]F. J. Himpsel and J. E. Ortega, Phys. Rev. B **46**, 9719 (1992).

[37]G. J. Mankey, R. F. Willis, and F. J. Himpsel, Phys. Rev. B **47**, 190 (1993).

[38]F. J. Himpsel, Phys. Rev. B **43**, 13 394 (1991).

[39]G. Bastard, *Wave Mechanics Applied to Semiconductor Heterostructures* (Les Editions de Physique, Les Ulis, France, 1988), Chap. III.

[40]By amplitude modulation, one obtains the sum and the difference between the carrier frequency (k_{edge}) and the modulation frequency (k_{env}). However, $\pm k_{\text{env}}$ are equivalent in Eq. (1) due to time-reversal symmetry.

[41]N. V. Smith, Rep. Prog. Phys. **51**, 1227 (1988).

[42]P. M. Echenique and J. B. Pendry, Prog. Surf. Sci. **32**, 111 (1990).

[43]P. D. Loly and J. B. Pendry, J. Phys. C **16**, 423 (1983).

[44]P. T. Coleridge and I. M. Templeton, Phys. Rev. B **25**, 7818 (1982).

[45]E. Eastman, J. A. Knapp, and F. J. Himpsel, Phys. Rev. Lett **41**, 825 (1978); J. A. Knapp, F. J. Himpsel, and D. E. Eastman, Phys. Rev. B **19**, 4952 (1979).

[46]G. V. Hansson and S. A. Flodström, Phys. Rev. B **18**, 1572 (1978).

[47]Yi Li and K. Baberschke, Phys. Rev. Lett. **68** 1208 (1992).

[48]F. Huang, M. T. Kief, G. J. Mankey, and R. F. Willis, J. Appl. Phys. (to be published); see also C. M. Schneider, P. Bressler, S. Schuster, J. Kirchner, J. J. de Miguel, and R. Miranda, Phys. Rev. Lett. **64**, 1059 (1990); G. J. Mankey, M. T. Kief, and R. F. Willis, J. Vac Sci. Technol A **9**, 1595 (1991).

[49]A. Santoni and F. J. Himpsel, Phys. Rev. B **43**, 1305 (1991); the bands shown in Fig. 6 for Fe are from J. Callaway and C. S. Wang, Phys. Rev. B **16**, 2095 (1977).

[50]Y. Suzuki, T. Katayama, S. Yoshida, K. Tanaka, and K. Sano, Phys. Rev. Lett. **68**, 3355 (1992).

[51]The phase shifts depend on the reference plane. We use the plane halfway between atomic layers. To rationalize the phase shifts for the band edge at X_4' one may consider the corresponding antibonding, p_z-like wave function at the zone boundary. It has nodes at the atomic planes and maxima in between, reversing its sign every atomic layer. The maxima correspond to a phase shift of zero. The situation is reversed either going to the zone center, or going to a bonding (s-like) state. Here, one has nodes instead of maxima in the reference plane between the atomic layers, corresponding to a phase shift of $\pm\pi$.

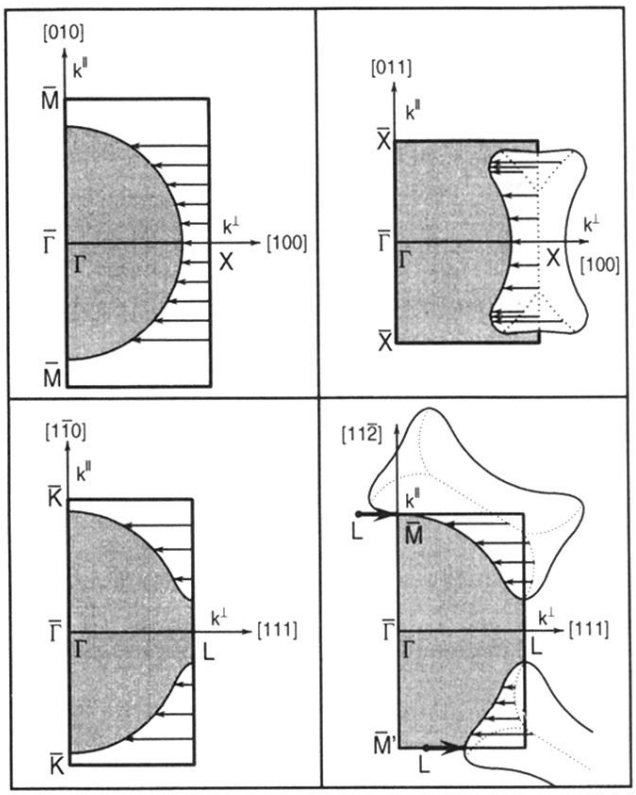

FIG. 8. Summation over oscillation periods for quantum-well states at the Fermi level in Cu(100) and Cu(111) films (top and bottom, respectively). The arrows represent the wave vectors of the envelope wave functions that determine the magnetic coupling period. They point from s,p band edges (dotted lines) to the Fermi surface. For Cu(100), the period near $k^{\parallel}=0$ dominates, whereas for Cu(111) there are no quantum-well states at $k^{\parallel}=0$ and a variety of periods at other $k^{\parallel}$.